Cycle-Dependent Degradation of Lithium-Ion Battery State of Health Under Normal, High-Rate, and Thermal Stress Conditions: A Dynamic Simulation Study

RAMALAN ABUBAKAR[1*], ABDULLAHI ZAKARI[2]
[1]*Department of Physics, University of Abuja, Abuja, Nigeria*
[2]*Department of Physics with Electronics, Air Force Institute of Technology (AFIT), Kaduna, Nigeria*
**Corresponding author: Ramalan Abubakar*

Abstract- Battery state of health (SOH) degradation is a critical factor in the life and reliability of lithium-ion batteries in electric vehicles, portable electronic devices, and grid storage systems. Understanding how different loading conditions affect capacity degradation and internal resistance increase is essential for developing battery management systems and predicting battery life. In this study, we developed a dynamic degradation model based on OpenModelica and simulated the SOH changes over the number of cycles under three conditions: normal charge/discharge cycles, high-current loading, and thermal loading. This model accounted for capacity degradation and resistance increase using linear degradation-rate parameters based on empirically determined trends. We simulated 1000 charge/discharge cycles and tracked the changes in SOH, capacity, usable energy, and coulombic efficiency. The results showed that SOH remained highest under normal charge/discharge conditions, at 80.0% after 1000 cycles, exceeding the usual end-of-life criterion throughout the simulation. Under high load, capacity degradation progressed most rapidly, with SOH decreasing to 40.0% after 1000 cycles. Under thermal load, the increase in internal resistance was most pronounced (0.22 Ω after 1000 cycles, a 120% increase from baseline), with SOH falling below the 80% threshold after 500 cycles. After 1000 cycles, usable energy decreased by 20.0% under normal operation, 40.0% under thermal load, and 60.0% under high load. This study shows that OpenModelica provides an effective dynamic simulation framework for battery aging analysis and life prediction, and that high discharge currents and high temperatures, despite their different characteristics, pose significant quantitative risks to battery life.

Keywords: lithium-ion battery; state of health; capacity fade; internal resistance; battery degradation; OpenModelica; cycle life; end-of-life prediction.

I. INTRODUCTION

Lithium-ion batteries are used as main batteries in electric vehicles, household appliances, and stationary storage systems due to their characteristics such as higher energy density, lower self-discharge, and longer life compared to conventional technologies [1]. However, their capacity decreases with use, internal resistance increases, and performance gradually declines. In most applications, a battery is considered obsolete when its state of health—i.e., the current capacity divided by the initial capacity—falls below 80% [2]. Therefore, accurate estimation of state changes and the number of charge cycles until end of life is essential for the design, warranty assessment, and overall life planning of battery management systems.

Battery aging results from a complex interplay of electrochemical reactions driven by physical and thermal stress. The main causes of capacity loss are lithium losses due to growth of the solid electrolyte interphase (SEI) film, lithium deposition on the negative electrode, and dissolution of the active material [3]. Internal resistance increases due to factors such as thickening of the SEI, poor contact between active material particles, and decomposition of the electrolyte [4]. These processes accelerate particularly strongly under two conditions: high discharge currents and high temperatures. Repeated charging and discharging with high currents pushes lithium into and out of the material, creating physical stresses that facilitate lithium deposition on the negative electrode and accelerate SEI formation [5]. At high temperatures, the decomposition reaction of the electrolyte becomes more active, increasing the

© AUG 2026 | IRE Journals | Volume 10 Issue 2 | ISSN: 2456-8880
DOI: https://doi.org/10.64388/IREV10I2-1722676

growth rate of the SEI and increasing resistance even under mild cycling conditions [6].

To study battery aging, computer simulations offer a practical and efficient means of analyzing a wide range of conditions without conducting long-term experiments. In particular, empirical degradation models are simple methods that use values calibrated from experimental data to calculate capacity loss and resistance increase as functions of cycle number, and can be readily implemented in a simulation environment using mathematical formulas [7]. OpenModelica is a free open-source platform based on the Modelica programming language that allows the easy creation of dynamic system models, and has recently been used for simulations of electrochemical energy storage [8, 9].

In this study, we used OpenModelica to create a battery aging model and simulate the change in battery state over 1000 charge–discharge cycles under three conditions: normal operation, high load, and thermal load. We measured capacity, internal resistance, usable energy, and coulombic efficiency, and predicted the number of cycles to end of life for each scenario. Based on these results, we compared the impact of cycling load on battery life.

II. MODEL DEVELOPMENT

2.1 Degradation Model Formulation

Battery degradation was modelled using linear empirical equations for capacity fade and internal resistance growth as functions of cumulative cycle number N. This formulation is consistent with the linear degradation regime commonly observed in lithium-ion batteries during the majority of their operational lifetime prior to the onset of accelerated end-of-life degradation [7]. The governing equations are:

$C(N) = C_0 \times (1 - \alpha\_cap \times N)$

$R(N) = R_0 \times (1 + \beta\_res \times N)$

where C_0 is the initial capacity (C), R_0 is the initial internal resistance (Ω), α_cap is the capacity fade rate per cycle, and β_res is the resistance growth rate per cycle. State of health, usable energy, and coulombic efficiency were derived as:

$SOH(N) = C(N) / C_0 \times 100\%$

$E\_usable(N) = C(N) \times V\_nom$

$\eta(N) = 100 \times (1 - 0.0001 \times N)$

Cycle number N evolved according to dN/dt = 1.

2.2 Scenario Parameters

Three degradation scenarios were defined. In the Normal Cycling scenario, capacity fade rate and resistance growth rate were set to low values representative of standard-rate discharge at room temperature. In the High-Rate Stress scenario, both rates were increased threefold and 2.7-fold respectively, reflecting the accelerated mechanical and electrochemical degradation associated with high-current cycling. In the Thermal Stress scenario, the capacity fade rate was set to an intermediate value while the resistance growth rate was set to the highest value across all scenarios, reflecting the dominant role of elevated temperature in driving SEI growth and resistance increase. Table 1 summarises the full parameter set.

Table 1. OpenModelica model parameters for the three degradation scenarios.

Scenario	C_0 (C)	R_0 (Ω)	α_cap	β_res	V_nom (V)	N
Normal Cycling	3600	0.10	0.0002	0.0003	3.7	1000
High-Rate Stress	3600	0.10	0.0006	0.0008	3.7	1000
Thermal Stress	3600	0.10	0.0004	0.0012	3.7	1000

2.3 Model Assumptions

The following assumptions apply: (1) degradation rates are constant throughout the simulation and do not accelerate at end of life; (2) capacity fade and resistance growth are independent and do not interact; (3) nominal voltage is constant at 3.7 V; (4) temperature effects are captured implicitly through the choice of degradation-rate parameters rather than explicitly through an Arrhenius thermal model; (5) the model compares relative degradation trends across scenarios rather than predicting the absolute lifetime of a specific commercial cell.

2.4 Simulation Setup

All simulations were executed in OpenModelica OMEdit from cycle 0 to cycle 1000 with 1000 output

© AUG 2026 | IRE Journals | Volume 10 Issue 2 | ISSN: 2456-8880
DOI: https://doi.org/10.64388/IREV10I2-1722676

intervals. Results were exported as CSV files and post-processed in Python for figure generation and end-of-life (EOL) cycle prediction.

III. RESULTS AND DISCUSSION

3.1 State of Health Evolution

Figure 1 shows SOH as a function of cycle number for all three scenarios, with the conventional 80% EOL threshold and a 60% critical threshold marked for reference. Normal cycling exhibited the slowest SOH decline, reaching exactly 80.0% at cycle 1000 and remaining above the EOL threshold throughout the simulation. Thermal stress crossed the 80% threshold at cycle 500, while high-rate stress reached EOL at cycle 334, the earliest of the three scenarios and less than one third of the normal cycling lifetime.

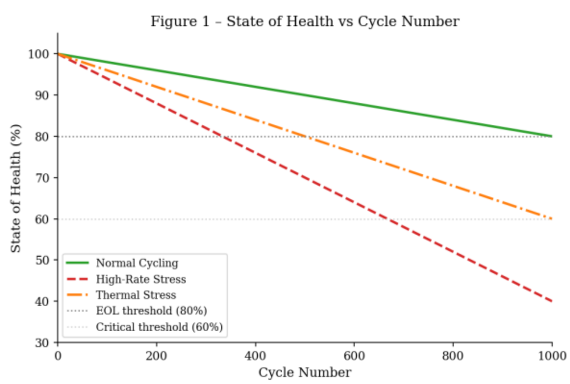

Figure 1. Simulated state of health versus cycle number for normal cycling, high-rate stress, and thermal stress scenarios. Dashed lines indicate the 80% EOL and 60% critical SOH thresholds.

The linear SOH trajectories reflect the constant degradation-rate parameters in the model. In reality, battery degradation often exhibits a two-stage profile with a linear phase followed by accelerated decline near end of life. The linear model captures the dominant mid-life degradation regime and is appropriate for comparative analysis across scenarios.

3.2 Capacity Fade

Figure 2 shows capacity as a function of cycle number. All three scenarios began with an identical initial capacity of 3,600 C. By cycle 1000, capacity had declined to 2,880 C (normal), 2,160 C (thermal), and 1,440 C (high-rate), representing losses of 20%, 40%, and 60% respectively. The high-rate stress scenario exhibited the steepest capacity decline throughout the simulation, consistent with the dominant role of mechanical degradation and lithium plating in capacity-limiting mechanisms under high-current operation.

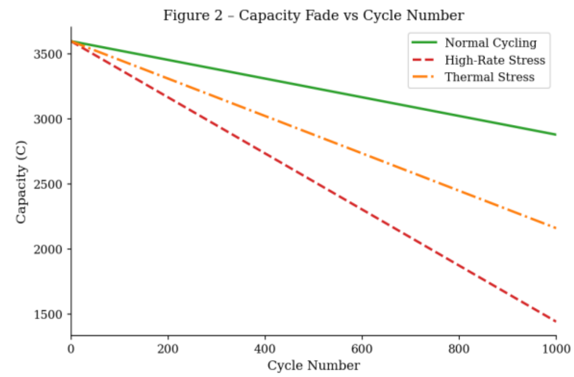

Figure 2. Simulated capacity fade versus cycle number for all three scenarios.

3.3 Internal Resistance Growth

Figure 3 shows internal resistance growth over 1000 cycles. The thermal stress scenario produced the highest final resistance (0.22 Ω), representing a 120% increase from the initial value of 0.10 Ω. High-rate stress reached 0.18 Ω (80% increase) and normal cycling reached 0.13 Ω (30% increase). The thermal stress scenario exhibiting higher resistance growth than high-rate stress, despite its intermediate capacity fade rate, reflects the specific sensitivity of SEI growth and electrolyte decomposition to temperature. This divergence between capacity fade ranking and resistance growth ranking is a key finding of the study: the most damaging stress condition depends on which performance metric is prioritised.

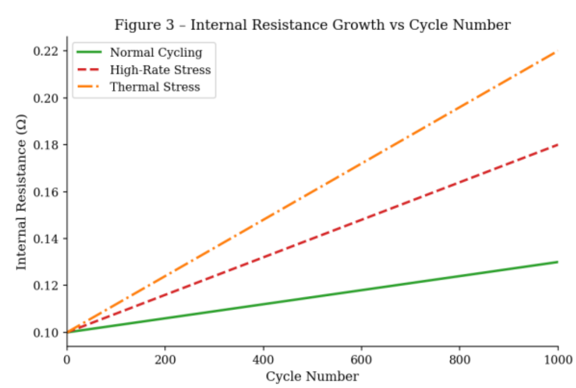

Figure 3. Simulated internal resistance growth versus cycle number for all three scenarios.

3.4 Usable Energy Decline

Figure 4 shows usable energy over the cycling period. Normal cycling retained 10,656 J at cycle 1000 from an initial 13,320 J, a retention of 80.0%. Thermal stress retained 7,992 J (60.0% retention) and high-rate stress retained only 5,328 J (40.0% retention). Since usable energy is directly proportional to capacity in this model, the energy-decline curves mirror the capacity fade profiles. From a practical standpoint, a battery under high-rate stress would deliver less than half the energy of a normally cycled battery by cycle 1000, with significant implications for electric vehicle driving range and backup power system runtime.

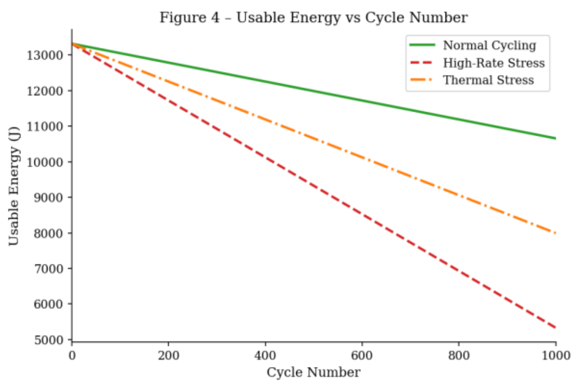

Figure 4. Simulated usable energy versus cycle number for all three scenarios.

3.5 Coulombic Efficiency

Figure 5 shows coulombic efficiency over the cycling period. All three scenarios follow the same efficiency trajectory, since coulombic efficiency was modelled as a function of cycle number independent of stress condition, declining from 100% to 90% over 1000 cycles. This reflects the gradual increase in parasitic side reactions common to all lithium-ion battery chemistries during cycling. Future model refinements could differentiate efficiency decay rates between scenarios to reflect the stress-specific enhancement of side reactions.

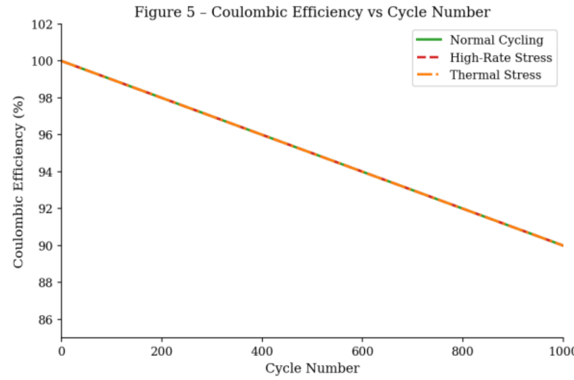

Figure 5. Simulated coulombic efficiency versus cycle number for all three scenarios.

3.6 SOH and Resistance at Cycle Milestones

Figures 6 and 7 present grouped bar charts comparing SOH and internal resistance at cycle milestones of 200, 400, 600, 800, and 1000. These visualisations highlight how performance separation between scenarios widens progressively with cycling. At cycle 200, the SOH difference between normal and high-rate stress is 12 percentage points. By cycle 600, this gap has grown to 36 percentage points, and by cycle 1000 it reaches 40 percentage points. The resistance comparison in Figure 7 similarly shows thermal stress pulling progressively ahead of the other scenarios in resistance accumulation from early in the cycling period.

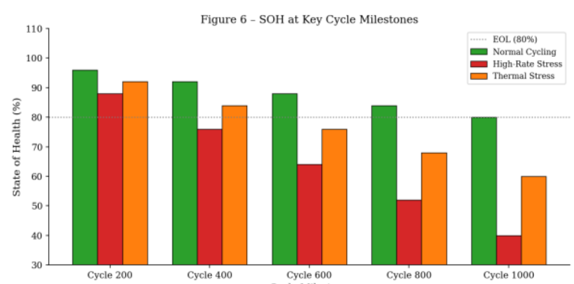

Figure 6. Simulated SOH at cycle milestones of 200, 400, 600, 800, and 1000 for all three scenarios. The dashed line indicates the 80% EOL threshold.

© AUG 2026 | IRE Journals | Volume 10 Issue 2 | ISSN: 2456-8880
DOI: https://doi.org/10.64388/IREV10I2-1722676

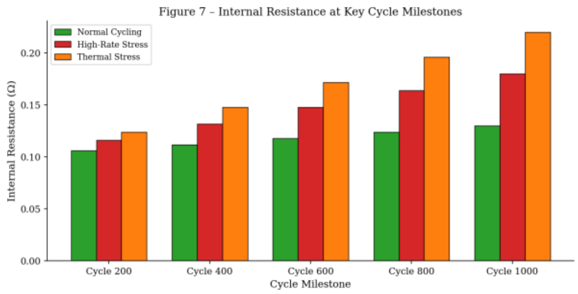

Figure 7. Simulated internal resistance at cycle milestones for all three scenarios.

3.7 End-of-Life Cycle Prediction

Figure 8 presents the predicted EOL cycle number for each scenario at the 80% SOH threshold. Normal cycling remained above the threshold throughout the 1000-cycle simulation, indicating a predicted operational lifetime exceeding 1000 cycles. Thermal stress crossed the threshold at cycle 500, and high-rate stress at cycle 334. Expressed as a fraction of the normal cycling lifetime, thermal stress delivers approximately 50% of the expected cycle life, while high-rate stress delivers only 33.4%. These results quantify the severe lifetime penalty associated with high-rate operation and underscore the importance of rate-limiting strategies in battery management systems for applications where longevity is prioritised over charge speed.

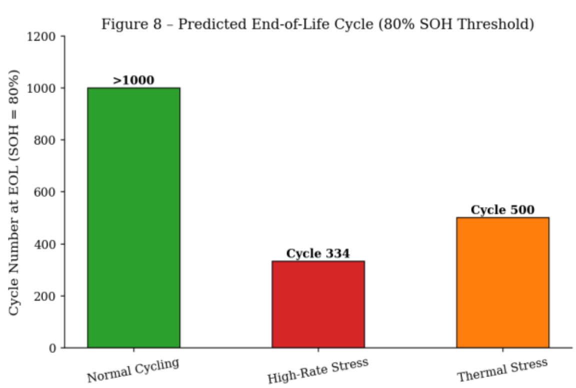

Figure 8. Predicted end-of-life cycle number at the 80% SOH threshold for each scenario.

3.8 Summary of Results

Table 2. Summary of simulation results at cycle 1000 and predicted EOL cycle numbers.

Scenario	SOH (%)	C_cap (C)	R_int (Ω)	E_use (J)	EOL	η (%)
Normal Cycling	80.00	2,880	0.130	10,656	>1000	90.00
High-Rate Stress	40.00	1,440	0.180	5,328	334	90.00
Thermal Stress	60.00	2,160	0.220	7,992	500	90.00

3.9 Physical Interpretation and Design Implications

The simulation results are in agreement with well-known principles of the degradation mechanisms of lithium-ion batteries. The main reasons for accelerated capacity degradation under high load are enhanced lithium deposition and mechanical stress, which lead to cracks in the active material particles. These two factors increase irreversible lithium loss and reduce intercalation capacity. The model depicts this with a high α_cap value, which leads to a sharp drop in SOH and the fastest attainment of EOL.

Thermal stress, by contrast, mainly accelerates growth of the SEI layer and decomposition of the electrolyte. These are kinetic processes whose reaction rates are strongly influenced by temperature and are described by Arrhenius-type behaviour. This is therefore expressed more as an increase in resistance than as an immediate loss of capacity, and for this reason the β_res value is set higher in the thermal-load scenario. In practice, batteries under thermal load appear to maintain capacity longer than batteries under high load, even though supply capability and energy efficiency decline as internal resistance gradually increases.

From the perspective of battery management system (BMS) development, three lessons can be drawn from these results. First, controlling the discharge rate is the most effective way to extend cycle life, as high discharge rates reduce the expected life to one third of that under normal cycling. Second, even in applications where capacity maintenance is the top priority, effective thermal management is essential to keep internal resistance low and preserve performance. Third, SOH alone is not a sufficient indicator of battery condition — especially under thermal load, the true extent of degradation remains undetected unless internal resistance is monitored alongside capacity.

IV. LIMITATIONS

The current model uses a linear degradation rate and does not represent the accelerated end-of-life degradation often observed in lithium-ion batteries once SOH drops below approximately 80%. The degradation-rate parameters are not based on specific experimental cycle data and should be considered representative values for comparative simulation rather than predictive values calibrated for a specific battery system. The model does not differentiate between individual degradation mechanisms such as SEI film growth, lithium deposition, and particle cracking, and does not treat temperature as an explicit state variable. Coulombic efficiency is modelled identically across all scenarios, representing a further simplification. Future work should introduce a nonlinear degradation model, incorporate temperature dependence via the Arrhenius law, add mechanism-specific degradation terms, and pursue experimental verification using measured cycle data from commercially available cells.

V. CONCLUSION

In this study, we developed and applied a dynamic degradation model based on OpenModelica to simulate the change in state of a lithium-ion battery over 1000 charge–discharge cycles under three conditions: normal charge–discharge cycling, high-power loading, and thermal loading. The core of the model lies in the treatment of capacity loss and internal resistance increase using linear, empirically founded rate equations, enabling a detailed comparison of degradation trajectories across the three scenarios and a theoretical prediction of battery life.

The simulation results were clear and revealed three physically plausible outcomes. Under normal charge–discharge conditions, SOH remained above the 80% end-of-life threshold over all 1000 cycles, with a final SOH of 80.0% and an internal resistance of 0.13 Ω. Under high-power load, capacity loss was drastic, dropping to 40.0%, and the service-life limit was exceeded after only 334 cycles — one third of the service life under normal conditions. Thermal stress led to a sharp increase in internal resistance to 0.22 Ω, a 120% increase, with the battery reaching its service-life limit after 500 cycles. After 1000 cycles, usable energy decreased by 20% under normal conditions, 40% under thermal load, and 60% under high-rate load.

In short, rapid discharge and elevated temperature represent distinct and quantitatively significant threats to battery life: rapid discharge appears to be the dominant cause of capacity loss, while thermal load is the dominant cause of resistance increase. This work demonstrates that OpenModelica is an effective platform for dynamic simulation of battery aging, and proposes a modelling framework useful for battery management system development, lifetime prediction, and charge/discharge protocol optimisation.

REFERENCES

[1] Tarascon, J.M.; Armand, M. (2001). Issues and challenges facing rechargeable lithium batteries. Nature, 414(6861), 359–367.

[2] Broussely, M.; Biensan, P.; Bonhomme, F.; Blanchard, P.; Herreyre, S.; Nechev, K.; Staniewicz, R.J. (2005). Main aging mechanisms in Li ion batteries. Journal of Power Sources, 146(1–2), 90–96.

[3] Vetter, J.; Novák, P.; Wagner, M.R.; Veit, C.; Möller, K.C.; Besenhard, J.O.; Winter, M.; Wohlfahrt-Mehrens, M.; Vogler, C.; Hammouche, A. (2005). Ageing mechanisms in lithium-ion batteries. Journal of Power Sources, 147(1–2), 269–281.

[4] Barré, A.; Deguilhem, B.; Grolleau, S.; Gérard, M.; Suard, F.; Riu, D. (2013). A review on lithium-ion battery ageing mechanisms and estimations for automotive applications. Journal of Power Sources, 241, 680–689.

[5] Ecker, M.; Nieto, N.; Käbitz, S.; Schmalstieg, J.; Blanke, H.; Warnecke, A.; Sauer, D.U. (2014). Calendar and cycle life study of Li(NiMnCo)O2-based 18650 lithium-ion batteries. Journal of Power Sources, 248, 839–851.

[6] Arrhenius, S. (1889). Über die Reaktionsgeschwindigkeit bei der Inversion von Rohrzucker durch Säuren. Zeitschrift für physikalische Chemie, 4(1), 226–248.

[7] Saha, B.; Goebel, K.; Poll, S.; Christophersen, J. (2009). Prognostics methods for battery health monitoring using a Bayesian framework. IEEE Transactions on Instrumentation and Measurement, 58(2), 291–296.

[8] Fritzson, P. (2014). Principles of Object-Oriented Modeling and Simulation with Modelica 3.3. IEEE Press / Wiley.

[9] Zubieta, L.; Bonert, R. (2000). Characterization of double-layer capacitors for power electronics applications. IEEE Transactions on Industry Applications, 36(1), 199–205.